PrRu$_2$Si$_2$: A giant anisotropic induced magnet with a singlet crystal-field ground state

A. M. Mulders

Interfacultair Reactor Instituut, Delft University of Technology, 2629 JB Delft, The Netherlands

A. Yaouanc and P. Dalmas de Réotier

Commissariat à l'Energie Atomique, Département de Recherche Fondamentale sur la Matière Condensée,
Service de Physique Statistique, Magnétisme et Supraconductivité, F-38054 Grenoble cedex 9, France

P. C. M. Gubbens and A. A. Moolenaar

Interfacultair Reactor Instituut, Delft University of Technology, 2629 JB Delft, The Netherlands

B. Fåk and E. Ressouche

Commissariat à l'Energie Atomique, Département de Recherche Fondamentale sur la Matière Condensée,
Service de Physique Statistique, Magnétisme et Supraconductivité, F-38054 Grenoble cedex 9, France

K. Prokeš, A. A. Menovsky, and K. H. J. Buschow

van der Waals-Zeeman Laboratorium, Universiteit van Amsterdam, 1018 XE Amsterdam, The Netherlands

The magnetic properties of PrRu$_2$Si$_2$ have been investigated experimentally by specific heat, single-crystal magnetization, ^{141}Pr Mössbauer and muon spectroscopies, neutron powder diffraction, and inelastic neutron scattering, leading to the determination of its zero-field phase diagram and its crystal electric-field energy levels below 40 meV. PrRu$_2$Si$_2$ undergoes a magnetic phase transition at $T_N \simeq 16$ K to an axial incommensurate sine-wave magnetic structure characterized by a wave vector $\tau = (0.133, 0.133, 0)$, followed by a first-order phase transition at $T_C \simeq 14.0$ K to an axial ferromagnetic structure. The lowest crystal electric-field states are the two singlets $|\Gamma_{t1}^{(1)}\rangle$ and $|\Gamma_{t2}\rangle$ separated by 2.25 meV. The low-temperature properties are described by a Hamiltonian identical to that of an Ising system with a transverse magnetic field. Since the ratio of the exchange energy to the energy splitting between the singlets is sufficiently large, it exhibits spontaneous magnetization. The nature of the two singlet states explains the giant magnetic anisotropy. The random-phase approximation predicts the value of the high-field magnetization but yields a low-field magnetization too small by $\sim 15\%$. Possible application of our results to uranium intermetallic compounds is pointed out. [S0163-1829(97)06138-9]

I. INTRODUCTION

Magnetic anisotropy is one of the most interesting and important subjects in magnetism. Ternary compounds RM_2X_2 (R = rare earth or actinide, $M = 3d$, $4d$, or $5d$ transition metal, and X = Si or Ge) with the tetragonal ThCr$_2$Si$_2$-type structure exhibit large magnetic anisotropy. Among these compounds, large anisotropy has been reported in Pr compounds (see Table 1 of Ref. 1 and Ref. 2). The largest measured anisotropy has been found for PrRu$_2$Si$_2$: its anisotropy field is $\simeq 400$ T.[1] This giant anisotropy is unexplained. It has been suggested that hybridization-induced anisotropy and/or anisotropy exchange interaction play a significant role.[1] This compound was believed to present only one magnetic phase transition to a ferromagnetic state[3] at $T_C = 14$ K. Only the Pr ions contribute to the magnetic properties of the compound.

Interestingly enough we note that Pr^{3+} has a $^3H_4$ Hund's rule ground multiplet as U^{4+} which is the usually assumed ionization state of uranium in intermetallics such as the well studied URu$_2$Si$_2$ heavy fermion compound.[4]

In this paper we report a study of the static magnetic properties of PrRu$_2$Si$_2$ using macroscopic and microscopic

experimental techniques. The organization of the paper is as follows. In Sec. II, we present our experimental results. Section III is devoted to the determination of the low-energy crystal electric-field (CEF) level scheme and to the analysis of the magnetic properties using either the molecular-field or random-phase approximation. In the last section we discuss our results. In the Appendix we list the eigenvalues and associated eigenstates of the CEF Hamiltonian.

II. EXPERIMENTAL RESULTS

The measurements have been performed on polycrystalline samples, except for the magnetization and muon spin relaxation measurements, which were carried out on single crystals.

A. Specific heat

The temperature dependence of the magnetic specific heat of PrRu$_2$Si$_2$, measured at temperatures ranging from 4.3 to 67 K, is presented in Fig. 1. The lattice and conduction electron contributions have been estimated from measurements on LaRu$_2$Si$_2$ and are subtracted from the raw PrRu$_2$Si$_2$
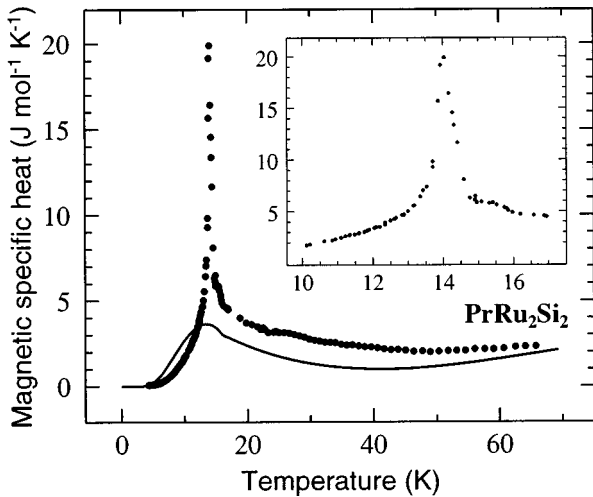
FIG. 1. Temperature dependence of the magnetic specific heat of PrRu$_2$Si$_2$. The lattice and conduction electron contribution has been estimated from measurements on LaRu$_2$Si$_2$ and subtracted from the raw PrRu$_2$Si$_2$ data. The solid line is the prediction of the molecular-field approximation with the energy levels shown in Fig. 11. The contribution of the two phase transitions is not taken into account.

data. A well-defined anomaly is observed at the ferromagnetic ordering temperature $T_C = 14.0$ K. In addition a weak anomaly is observed starting at ~ 16 K (see the inset of Fig. 1). As we will show in Secs. II D and II E, this anomaly corresponds to a second magnetic phase transition. In Fig. 2 we display the temperature dependence of the entropy computed from the magnetic specific-heat data. This entropy reaches $R\ln2$ at ~ 30 K, indicating that there are two levels of equal degeneracy populated below that temperature including the ground state.

B. Single-crystal magnetization

The magnetization measurements have been performed using a superconducting quantum interference device (SQUID) magnetometer. The data are shown in Fig. 3. They
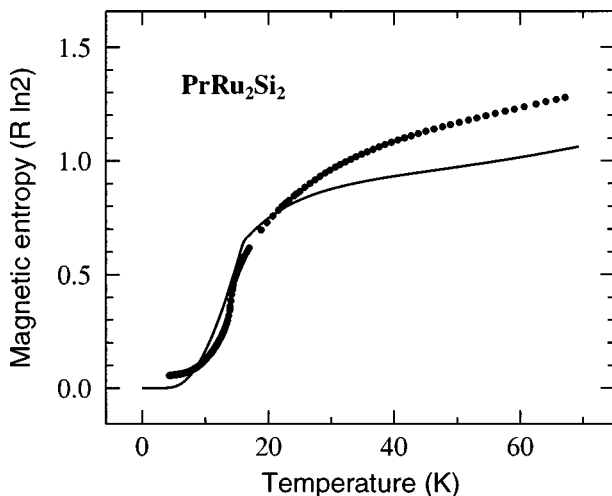

FIG. 2. Temperature dependence of the entropy computed from the specific heat presented in Fig. 1. The solid line corresponds to the model used in that figure.
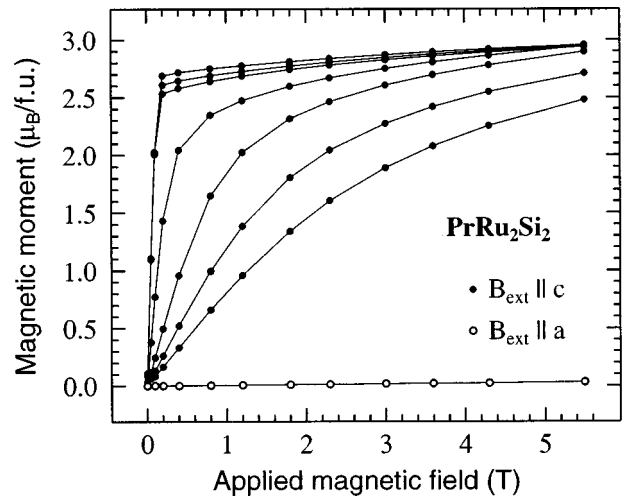

FIG. 3. Field dependence of the magnetization recorded on a single crystal of PrRu$_2$Si$_2$ with the magnetic field $\mathbf{B}_{ext}$ parallel to the c axis for different temperatures 4.5 K, 10.5 K, 12 K, 16 K, 20 K, 24 K, and 28 K (solid circles). For a given field, the higher the temperature, the lower the magnetization is. In addition we present data taken at 28 K with $\mathbf{B}_{ext}$ parallel to the a axis (open circles). The solid lines are guides to the eyes.

indicate that the bulk magnetic moment at 4.5 K is $2.69\mu_B$, in agreement with the previously reported result of $2.7\mu_B$.[1] We notice that even at a temperature twice the value of T_C the anisotropy is strong: Whereas in an applied magnetic field of 5.5 T the magnetization at 28 K is $2.5\mu_B$ when measured along the c axis, it is only $0.032\mu_B$ for the field applied along the a axis.

High-field magnetization measurements have been performed in fields up to 35 T. These measurements confirm the strong anisotropy of this compound. At 4.2 K, in an applied field of 35 T, the value of the magnetization measured along the c and a axes is $3.08\mu_B$ and $0.39\mu_B$, respectively.

C. ^{141}Pr Mössbauer spectroscopy

The ^{141}Pr Mössbauer measurements (145.4 keV nuclear transition) have been performed using a special counting technique. The current was directly integrated from the detector, instead of counting each single event.[5] All the spectra were measured with a CeF$_3$ source (initially 750 mCi) kept at 4.2 K, working with an acceleration-type spectrometer in sinusoidal mode. The velocity was calibrated with a ^{57}Co:Rh source and a α-Fe$_2$O$_3$ absorber at room temperature.

The ^{141}Pr Mössbauer spectra were recorded at temperatures from 4.2 to 25 K. The spectrum measured at 4.2 K is shown in Fig. 4. From the splitting of the absorbtion lines, a hyperfine field at the nuclear site of 281 T is deduced. This corresponds to a Pr $4f$ magnetic moment of $2.76\mu_B$ (see also Fig. 7). The small difference between this value and the value measured by magnetization is understood if we remember that the $5d$ electrons of any rare-earth ion contribute to the bulk magnetization. This $5d$ moment equals $\sim 0.1\mu_B$ and is oriented antiparallel to the $4f$ moment for a light rare-earth ion[6] as shown from x-ray magnetic circular dichroism measurements.[7]
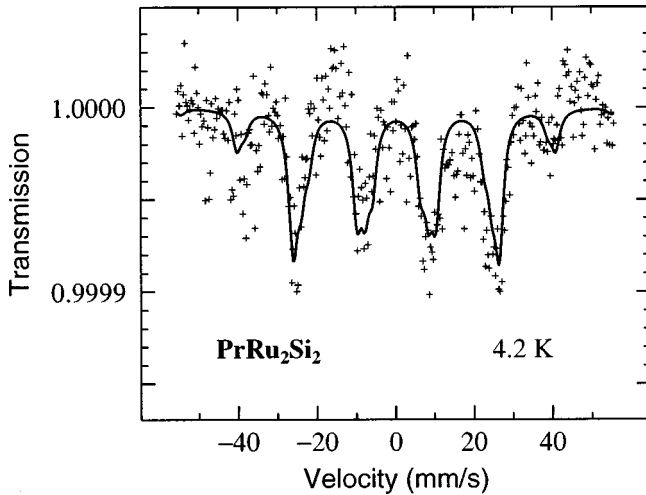
FIG. 4. ^{141}Pr Mössbauer spectrum of PrRu$_2$Si$_2$ recorded at 4.2 K. The solid line is a fit with the isomer shift and the hyperfine field as free parameters of which a Pr $4f$ moment of $2.76\mu_B$ is deduced.

D. Muon spectroscopy

Muon spin relaxation (μSR) spectroscopy has proved to be a very powerful tool for the investigation of magnetic phenomena. In this technique, polarized muons are implanted into a sample where their spins evolve in the local magnetic field until they decay.[8] The decay positron is emitted preferentially along the final muon spin direction; by collecting the positrons, we can reconstruct the time dependence of the muon spin polarization $P_Z(t)$. If the initial muon beam polarization and the local field are parallel, $P_Z(t)$ decreases exponentially in time with a relaxation rate $\lambda = 1/T_1$ where T_1 is the muon spin lattice relaxation time. λ exhibits a maximum at a magnetic phase transition.

The experiments have been carried out at the ISIS surface muon facility located at the Rutherford Appleton Laboratory (UK). Figure 5 shows $\lambda(T)$ recorded in an applied longitu-
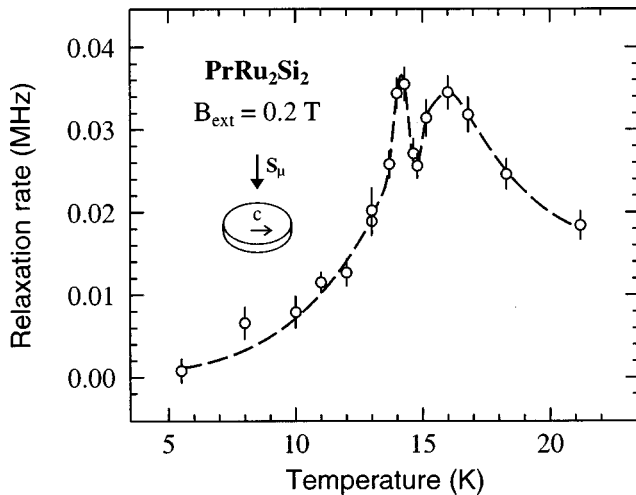

FIG. 5. Temperature dependence of the μSR longitudinal exponential relaxation rate measured on PrRu$_2$Si$_2$ with $B_{ext} = 0.2$ T. The initial muon polarization is perpendicular to the c axis. The critical temperatures of the two magnetic phase transitions are located at temperatures for which the relaxation rate exhibits extrema. The dashed line is a guide to the eyes.

dinal field of 0.2 T. This field is necessary to suppress the depolarization due to the ^{141}Pr nuclear magnetic moments, the effect of which is enhanced by the large hyperfine coupling constant and Van Vleck susceptibility.[9]

We will not discuss the μSR results in details. We only analyze the ones giving information about the magnetic phase diagram.

$\lambda(T)$ presents two extrema, one at $\sim$ 14 K and a second one at $\sim$ 16 K. This shows that, in addition to the phase transition at T_C, there is a second magnetic phase transition at $T_N \sim$ 16 K. Although it is difficult to detect T_N in the magnetic specific-heat data, muon spectroscopy clearly shows its signature.

E. Neutron powder diffraction

In order to further study the transition at T_N, we have performed neutron-powder-diffraction experiment in the temperature range 2–19 K. These experiments have been carried out in Grenoble at the Siloé reactor of the Commissariat à l'Energie Atomique on the DN5 linear multidetector diffractometer using an incident neutron wavelength of 2.487 Å. The data were refined using the MXD program.[10] The scattering lengths ($b_{Si} = 4.15$ fm, $b_{Pr} = 4.58$ fm, and $b_{Ru} = 7.03$ fm) were taken from Ref. 11, and the magnetic form factor of Pr^{3+} from Ref. 12. Owing to a possible preferential orientation, the calculated intensities were corrected using the March formula[13]

$$M_{hkl} = \left[f_{cor}\cos^2\alpha + \frac{\sin^2\alpha}{f_{cor}} \right]^{-3/2}, \qquad (1)$$

where M_{hkl} is a corrective factor for the calculated intensity, f_{cor} the fitted coefficient which reflects the importance of preferential orientation, and α the angle between the c axis and the hkl plane.

The indexation of the nuclear Bragg peaks in the paramagnetic state ($T = 19$ K) confirms unambiguously the ThCr$_2$Si$_2$-type structure for this compound (space group $I4/mmm$): (i) one Pr atom in the (0,0,0) site, (ii) two Ru atoms in the (0,1/2,1/4) and (1/2,0,1/4) sites, and (iii) two Si atoms in the (0,0,z) and (0,0,$\bar{z}$) sites. The fit of the integrated intensities gives no evidence for any mixing between the Ru and Si atoms. A quite good agreement (reliability factor $R = 0.059$) is obtained for $z_{Si} = 0.3634(24)$ and $f_{cor} = 1.114(20)$

The values of the f_{cor} and z_{Si} factors are, within the experimental uncertainty, temperature independent. All the recorded spectra are well described by our model as shown by the fact that the reliability factors are never larger than $R = 0.063$. The lattice parameters a and c are temperature independent. We find $a = 4.1864$ (2) Å and $c = 9.755$ (15) Å.

Between $T_N \sim$ 16.0 K and $T_C \sim$ 14.0 K, additional reflections can be identified as seen in Fig. 6. Note the intense reflection at small diffraction angle which only exists in the incommensurate phase. The new reflections, due to the onset of the magnetic order, can be indexed with a wave vector $\tau = (0.133,0.133,0)$ which is temperature independent. The magnetic moments of this sine-wave-modulated structure are parallel to the c axis with an amplitude of $1.8(1)\mu_B$ at 14.5 K. Besides these reflections, additional intensities appear on
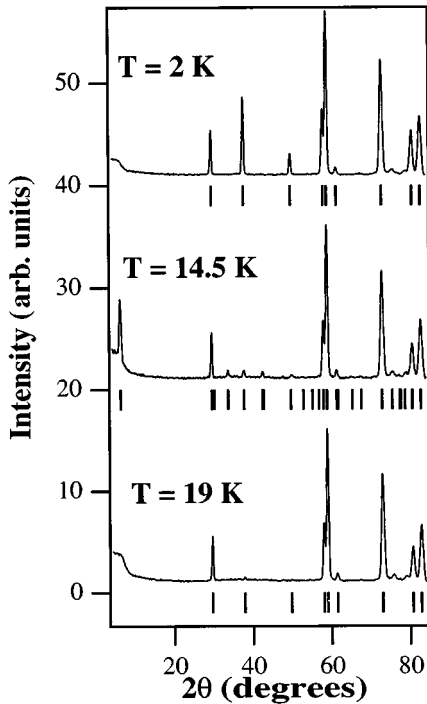
FIG. 6. Neutron-powder-diffraction patterns from paramagnetic ($T = 19$ K), incommensurate plus ferromagnetic ($T = 14.5$ K), and ferromagnetic ($T = 2$ K) phases of PrRu$_2$Si$_2$.

the nuclear Bragg reflections that can be accounted for by a ferromagnetic contribution with the magnetic moments along the c axis. At 14.5 K the ferromagnetic moment is $1.0(1)\mu_B$. The temperature dependence of the ferromagnetic magnetic moment and of the amplitude of the incommensurate modulation are presented in Fig. 7. The ratio of the intensities of the two magnetic components depends on the experimental
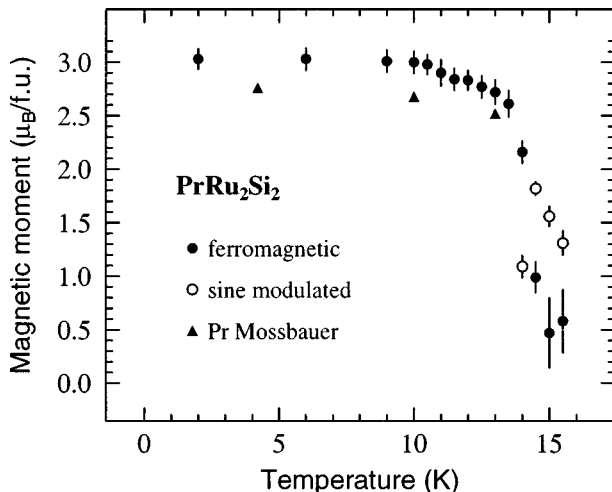

FIG. 7. Temperature dependence of the $4f$ magnetic moment measured by neutron diffraction in PrRu$_2$Si$_2$. Below 14 K an axial ferromagnetic structure is observed (solid circles). Between 14 and 16 K a second magnetic structure is observed characterized by an incommensurate sine-wave modulation with $\tau = (0.133,0.133,0)$ (open circles). In addition the $4f$ magnetic moment measured at three temperatures by ^{141}Mössbauer spectroscopy is presented (solid triangles). Both data sets show that the ferromagnetic transition at 14 K is first order.

procedure, i.e., spectra recorded in cooling down or in warming up the sample. This is a characteristic for a first-order transition at T_C. The values presented at Fig. 7 correspond to cooling down the sample from 19 K to 2 K.

Below T_C the sine-wave phase has disappeared and only the ferromagnetic contribution remains with a Pr $4f$ moment of $3.0(1)\mu_B$ at 2 K. Although this value is slightly larger than the one deduced from magnetization and Mössbauer measurements ($\sim 2.8\mu_B$), it is still reasonable taking into account the difficulty to measure precisely the intensity of the Bragg peaks in a textured powder sample. The temperature dependence of this moment as measured by neutron diffraction is plotted also in Fig. 7.

F. Inelastic neutron scattering

The inelastic-neutron-scattering (INS) method has been widely used to extract information on the energy-level scheme of rare-earth ions in intermetallic compounds. In favorable cases it allows us to observe directly the dipolar transitions between the CEF energy levels of the rare-earth ions. In order to simplify the analysis of the INS data the measurements are performed only in the paramagnetic phase. Since our specific-heat measurements[14] indicate that an CEF energy level is located at low energy, we have carried out the measurements on a sample with the Pr ions partly substituted by nonmagnetic La ions. The substitution is expected to depress the magnetic ordering temperature but not to drastically modify the CEF acting on the Pr ions. We have chosen La$_{0.5}$Pr$_{0.5}$Ru$_2$Si$_2$ because magnetization measurements show that it is still paramagnetic at 2 K.

The INS measurements have been performed in Grenoble with the DN6 time-of-flight spectrometer located at the Siloé reactor. Thermal neutrons of incident energy $E_i = 17$ meV were used to record spectra at 3.2 K, 18.3 K, 52 K, and 300 K. Additional scans at $E_i = 69$ meV were performed at temperatures 3.4 K and 52 K. The spectra were collected for scattering angles between 23° and 103°.

We have corrected the spectra for the background signal, yielding the total normalized response referenced to a vanadium standard. The angular dependence of the scattered intensity allowed us to separate unambiguously the magnetic contribution to the scattering (proportional to the square of the magnetic form factor, which decreases when the wave vector q increases) from the phonon contribution (proportional to q^2). As shown in Fig. 8 and Fig. 9, in the energy range 1–40 meV we have detected only two inelastic peaks corresponding to crystal-field excitations at 2.25(5) meV and 28.4(1) meV. The high-energy peak displays a clear temperature dependence as indicated in Fig. 10. While at 3.4 K the energy and the full width at half maximum are, respectively, 28.4(1) meV and 3.1(1) meV, at 52 K they are 27.7(1) meV and 3.8(1) meV, respectively. The thermal behavior of the high-energy peak is consistent with the presence of the low-energy CEF excitation (see Sec. III B).

III. ANALYSIS OF THE EXPERIMENTAL RESULTS

We will first write the Hamiltonian which should account for our experimental results and describe some of our data with the CEF part of this Hamiltonian. Then, using the com-
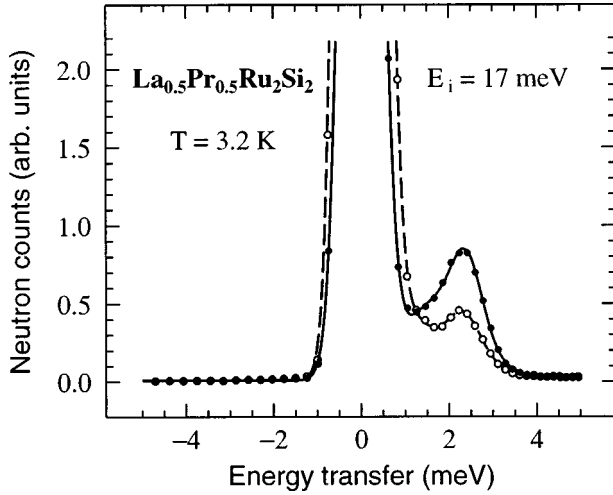
FIG. 8. Spectral response of $La_{0.5}Pr_{0.5}Ru_2Si_2$ recorded at $T = 3.2$ K for an incident neutron energy $E_i = 17$ meV. The solid and open circles are for measurements performed at average scattering angles of 25.5° and 95°, respectively. The scattering at small angles is dominated by the CEF transition. The lines are guides to the eyes.

plete Hamiltonian, we will attempt an analysis of our magnetic data, first in the framework of the molecular field approximation, then in the random-phase approximation. This latter analysis considers only the lowest two CEF levels.

A. Hamiltonian

The complete Hamiltonian used for describing the magnetic properties is written as the sum of three terms:

$$\mathcal{H} = \mathcal{H}_{CEF} + \mathcal{H}_{exch} + \mathcal{H}_Z. \qquad (2)$$

Using the equivalent-operator method and the z axis being parallel to the [001] direction, the CEF term $\mathcal{H}_{CEF}$ is written as

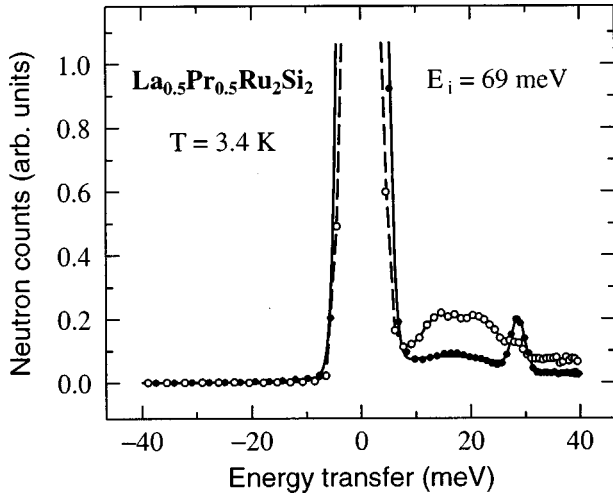FIG. 9. Spectral response of $La_{0.5}Pr_{0.5}Ru_2Si_2$ recorded at $T = 3.4$ K for an incident neutron energy $E_i = 69$ meV. The solid and full circles are for measurements performed at average scattering angles of 25.5° and 95°, respectively. The scattering at small angles is dominated by the CEF transition, whereas at 95° phonon excitations dominate the spectrum with a maximum intensity at $\sim$ 17 meV. The lines are guides to the eyes.
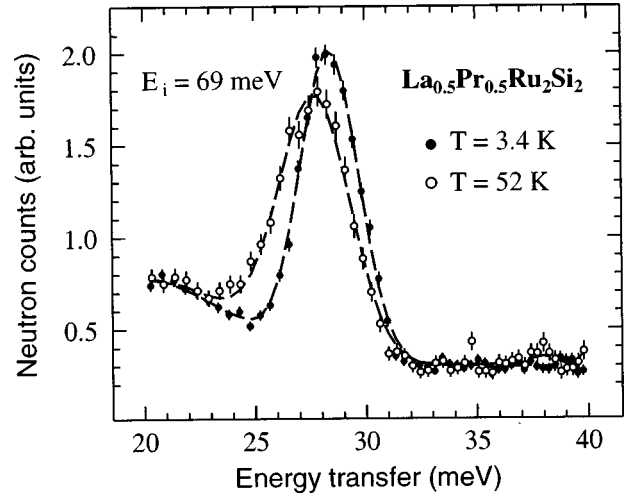

FIG. 10. Comparison of the spectral response of $La_{0.5}Pr_{0.5}Ru_2Si_2$ recorded at 3.4 K and 52 K with an incident neutron energy $E_i = 69$ meV and at scattering angle of 25.5°. We only display the data recorded in an energy-transfer window centered around the high-energy CEF transition. This comparison shows that both the energy and the full width at half maximum of the CEF transitions are temperature dependent. The dashed lines are guides to the eyes.

$$\mathcal{H}_{CEF} = B_2^0 O_2^0 + B_4^0 O_4^0 + B_4^4 O_4^4 + B_6^0 O_6^0 + B_6^4 O_6^4, \qquad (3)$$

where the O_l^m's are the Stevens-equivalent operators and B_l^m are CEF parameters.[15]

$\mathcal{H}_{exch}$ describes the magnetic exchange interaction between the Pr^{3+} total angular momenta **J** and $\mathcal{H}_Z$ accounts for the Zeeman coupling.

B. Crystal-field determination

We first consider the CEF part of $\mathcal{H}$. Its diagonalization provides the CEF eigenvalues and eigenstates, leading to the raising of the degeneracy of the $4f$ ground multiplet. For the Pr^{3+} ion ($J = 4$) in the tetragonal point group D_{4h}, the multiplet splits into five singlets ($\Gamma_{t1}^{(1)}$, $\Gamma_{t1}^{(2)}$, Γ_{t2}, Γ_{t3}, Γ_{t4}) and two doublets ($\Gamma_{t5}^{(1)}$, $\Gamma_{t5}^{(2)}$). The Γ_j's are the irreducible representations of the point group. The eigenvalues and associated eigenstates can be expressed analytically in terms of the B_l^m parameters. They are given in the Appendix.

The large magnetic moment observed at low temperature in combination with the specific-heat and INS data allows us to specify the nature and location of some of the CEF levels.

We first notice that at $T \ll T_C$ the magnetic moment is so large that the CEF ground state must contain the $|\pm 4\rangle$ states; i.e., it is either $|\Gamma_{t1}^{(1)}\rangle$, $|\Gamma_{t1}^{(2)}\rangle$, or $|\Gamma_{t2}\rangle$ (see the Appendix). $|\Gamma_{t1}^{(1)}\rangle$ is the ground state of $\mathcal{H}_{CEF}$ because it has the lowest energy (we have discarded the accidental case $b_1 = 0$). This state is a nonmagnetic singlet. It is known that a large magnetic moment can be generated at low temperature from a magnetic singlet only if there is at least one CEF energy level located at an energy comparable to the exchange energy.[16–18] Since $PrRu_2Si_2$ is an axial ferromagnet, the exchange field is proportional to a J_z matrix element. Therefore the first excited CEF state, $|first\rangle$, must be such that
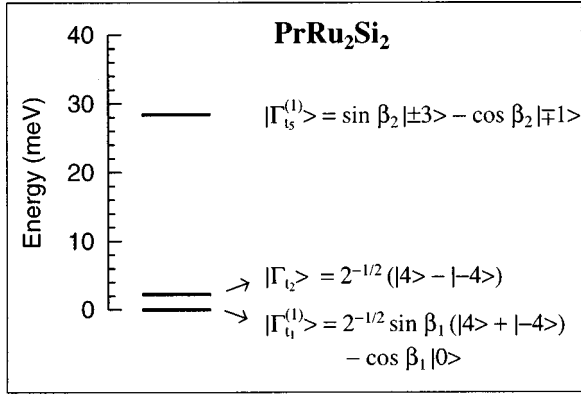
FIG. 11. Crystal-electric-field energy-level scheme of the Pr^{3+} ions in PrRu$_2$Si$_2$ deduced in this work. The inelastic neutron investigation did not detect any other states below 40 meV. The five states not mentioned in the figure are most likely located above 40 meV. They do not influence the magnetic properties at low temperature. The β_1 and β_2 values are near $\pi/2$.

$\langle\Gamma_{t1}^{(1)}|J_z|\text{first}\rangle$ is nonzero. The only possible first excited state is $|\Gamma_{t2}\rangle$ since the $|\Gamma_{t1}^{(2)}\rangle$ state is located at higher energy (see the Appendix).

The CEF dipolar transitions observed by INS are induced by the J_z, J_+, or J_- operators. The neutron cross section $I(i,f)$ between an initial state i and a final state f is given by

$$I(i,f)=I_0\left[\sin^2\theta|\langle i|J_z|f\rangle|^2+\frac{(2-\sin^2\theta)}{4}(|\langle i|J_+|f\rangle|^2\right.$$

$$\left.+|\langle i|J_-|f\rangle|^2)\right], \qquad (4)$$

where I_0 is a constant and θ the angle between the scattering vector and the quantization direction. Since $I(\Gamma_{t1}^{(1)},\Gamma_{t2})$ $=16I_0\sin^2\theta\sin^2\beta_1$, this transition is intense only if $\sin^2\beta_1$ is not too small. It corresponds to the peak seen at $\Delta=2.25(5)$ meV. The only other possible neutron transitions from the ground state are to the $|\Gamma_{t5}^{(1)}\rangle$ and $|\Gamma_{t5}^{(2)}\rangle$ states (see the Appendix). The $|\Gamma_{t5}^{(1)}\rangle$ state being the lowest in energy, we attribute the peak observed at 28.4(1) meV to the transition from the ground state to this state. We have $I(\Gamma_{t1}^{(1)},\Gamma_{t5}^{(1)})=$ $I_0(2-\sin^2\theta)(\sin\beta_1\sin\beta_2+\sqrt{5}\cos\beta_1\cos\beta_2)^2$. Since probably $|\sin\beta_1|\lesssim1$ (see Sec. III C), $I(\Gamma_{t1}^{(1)},\Gamma_{t5}^{(1)})\simeq$ $I_0(2-\sin^2\theta)\sin^2\beta_2$. Because the high-energy CEF excitation is intense, we infer a substantial value for $\sin^2\beta_2$.

Possible CEF levels below 28.4 meV which are invisible to the INS technique [i.e., $I(\Gamma_{t1}^{(1)},f)$ small] are not likely because their presence would strongly enhance the Schottky anomaly even below 67 K (see Sec. III C). The crystal-field-level scheme deduced from the analysis is drawn in Fig. 11.

We have observed that the high-energy neutron peak (28.4 meV) has temperature-dependent characteristics (see Fig. 10). This is easily understood because while at low temperature the observed peak is only produced by the neutron transition from the ground state $|\Gamma_{t1}^{(1)}\rangle$ to the $|\Gamma_{t5}^{(1)}\rangle$ state, at high temperature the ground and first excited states participate in the observed neutron transition. This explains the fact that at 52 K the observed peak is wider and located at lower energy than at low temperature.

In summary, the CEF ground state and first excitation state are singlet states well separated in energy from the other CEF states. Therefore the low-temperature magnetic properties of PrRu$_2$Si$_2$ should be understood by considering the Pr^{+3} ions as two-level systems interacting on a lattice. In the next section we use this level scheme to further analyze our data.

C. Analysis of the data in the molecular-field approximation

Both Trammell and Bleaney recognized a long time ago that exchange forces induce magnetic ordering in a singlet CEF ground state if these forces are strong enough.[16,17] An expression for the magnetization of the $4f$ electrons at $T=0$ is obtained in the molecular-field approximation:[17]

$$M_{4f}(T=0)=4g_J\mu_B\sin\beta_1\left[1-\tanh^2\left(\frac{\Delta}{2k_BT_C}\right)\right]^{1/2}, \qquad (5)$$

where g_J is the Landé factor ($g_J=4/5$ for Pr^{3+}), μ_B the Bohr magneton, k_B the Boltzmann constant, and Δ $=E_{t2}-E_{t1}^{(1)}$. Our measurements give $\Delta=2.25$ meV and $T_C=14$ K. The observed INS peak intensity as well as the size of the magnetic moment indicates a value of $\sin^2\beta_1$ close to 1. Using $\sin\beta_1=1$ and Eq. (5) we deduce the maximum value that $M_{4f}(T=0)$ can reach: $2.18\mu_B$. This is much lower than the experimental value of $2.8\mu_B$.

To explain the observed moment value within the molecular-field approximation, Δ should be reduced substantially or the magnetic ordering temperature should be drastically raised; i.e., we should have $\Delta/2k_BT_C=0.53$ instead of 0.93. The first possibility is excluded since an INS transition is clearly observed at 2.25 meV and also the entropy shows no sign of a singlet below ~20 K. The second possibility is also excluded since specific heat, μSR, and neutron diffraction indicate magnetic transitions at 14 and 16 K.

In addition, the shape of the magnetization curve as presented in Fig. 7 is more rectangular than a Brillouin curve. This is a signature of a first-order transition. In contrast to this, the molecular-field approximation predicts that the ferromagnetic transition is second order (see Fig. 12).

Although the molecular-field approximation does not provide a reasonable description of the low-field magnetization measurements, it should be useful to understand the specific heat data since they should be dominated by the effect of the CEF levels, i.e., by the Schottky anomaly. We do not attempt to describe the specific heat related to the magnetic phase transitions. The solid line in Fig. 1 represents the calculated specific heat with a singlet at $E_{t2}=2.25$ meV and a doublet at $E_{t5}^{(1)}=28.4$ meV. Below T_C the effect of the molecular field is taken into account. The related entropy curve is shown in Fig. 2. The discrepancy between the model and the experimental data is small, taking into account the fact that the magnetic phase transitions are not described. Note that an extra singlet between 2.25 and 28.4 meV yields a too large specific heat (and entropy). This is a strong indication that there are no other CEF levels below 40 meV, apart from the ones already identified (see Fig. 11).

The magnetic anisotropy measured at high field is controlled by the nature of the CEF energy levels and the Zeeman effect due to the field; i.e., the effect of the molecular
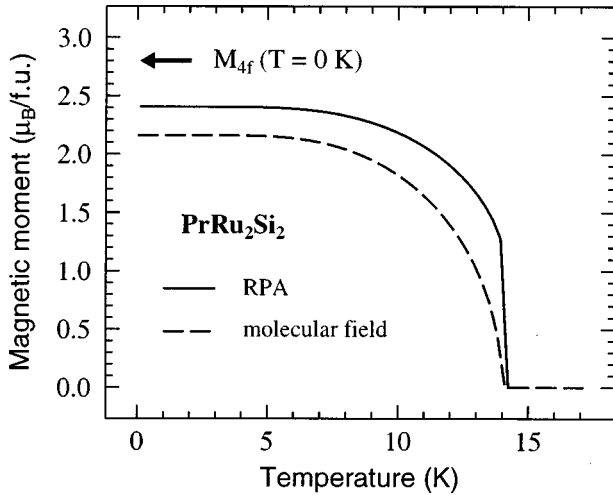
FIG. 12. Calculated magnetization curve in the molecular-field approximation (dashed line) and the random-phase approximation (solid line). The arrow indicates the value of the magnetic moment of the 4*f* electrons as deduced from magnetization and Mössbauer measurements.

field is small. Therefore the computation of the high-field anisotropy should be reliable. At 5.5 T we compute $2.87\mu_B$ and $0.03\mu_B$ for $\mathbf{B}_{ext}$ parallel and perpendicular to c, respectively. At 35 T we have $3.14\mu_B$ for $\mathbf{B}_{ext}$ parallel to c, which is very closed to the experimental value $(3.08\mu_B)$ and $0.19\mu_B$ for $\mathbf{B}_{ext}$ perpendicular to c which is twice as low as the experimental value, but this could be explained by a slight misalignment of the crystal which would have important consequences for a so strongly anisotropic crystal. These calculated values are then globally consistent with our data and the previously published results.[1]

D. Analysis of the magnetic properties in the random-phase approximation

We have just showed that the molecular-field approximation fails to provide a description of the low-field magnetization. Referring to previous works on singlet magnets,[19] this is not surprising.

Since the two singlets are close together, collective excitations of the singlet ground state take place.[20–23] These excitations are passed on from one atom to another, a process similar to that observed in spin waves. The most simple theory which attempts to account for these excitations is the random-phase approximation (RPA). In the paramagnetic state its Hamiltonian reduces to the Ising Hamiltonian in a transverse field. The energy spectrum of the excitations shows a dispersion with a minimum energy gap at $\mathbf{k} = 0$ (zone center). The shape of the dispersion and the size of the energy gap depend on the exchange strength and the relative temperature $k_B T/\Delta$. Reaching T_C from either above or below, the energy gap decreases towards zero. This reduction of the energy gap is an effective channel to depopulate the singlet ground state and therefore, in the RPA, T_C is reduced compared with the molecular-field approximation. Also the RPA magnetization curve is more rectangular due to this effect and the transition to the paramagnetic state becomes first order. In Fig. 12 we present its predictions using the formalism of Ref. 21. It provides a better description than the

molecular field approximation: It predicts that the transition is first order and yields a larger moment at low-temperature. But this moment is still $\sim$ 15 % smaller than observed.

IV. DISCUSSION

Our study has shown that the RPA of Ref. 20 gives a better description of the low temperature properties of $PrRu_2Si_2$ than the molecular-field approximation. We note that $k_B T_C$ is of the same order as Δ and strong correlations effects are hence expected. However, these effects are not sufficiently taken into account in the RPA. Since the CEF parameters of $PrRu_2Si_2$ are now well defined, this compound provides a good system to test theoretical predictions for these correlation effects. In addition, inelastic-neutron-scattering experiments on single crystals could reveal the nature of the dispersion.

We now discuss the phase diagram of $PrRu_2Si_2$. We first note that $NdRu_2Si_2$ exhibits the same magnetic structure below T_C and between T_C and T_N.[24] Only the values of T_C and T_N are different. This type of phase diagram, which has been found in many rare-earth-based intermetallics, has been successfully explained by Gignoux and Schmitt with a periodic field model taking into account the crystal-field anisotropy.[25] It appears that the exact boundaries of the magnetic phase diagram is determined by the real variation of the wave-vector-dependent exchange interaction and the crystal field.

In recent years the physics of uranium intermetallics has attracted much attention. The family of compounds with the $ThCr_2Si_2$ crystal structure is particularly interesting since it offers the possibility to study the effect of the hybridization of the f electrons with the $6d$ and p electrons in a systematic way.[26] Interestingly, the uranium $5f$ shell may have the same electronic structure as the Pr^{3+} $4f$ shell. The ground state and the first excited state may even be the same as in $PrRu_2Si_2$.[26] Therefore our results should help for the understanding of the origin of the large magnetic anisotropy found in some uranium compounds. Our work suggests that an effective crystal-field Hamiltonian could be an efficient method for the description of the anisotropy.

In the $ThCr_2Si_2$ crystal structure family, URu_2Si_2 is being studied intensively since it is a heavy-fermion superconductor. Its magnetic properties have been investigated with the Hamiltonian used for $PrRu_2Si_2$, treated in the molecular-field approximation.[27,4] Although URu_2Si_2 has a very small moment and $PrRu_2Si_2$ a large moment, our work indicates that the results of the molecular-field approximation should be taken with caution. Recently Sikkema *et al.* have analyzed the properties of URu_2Si_2 with a mean-field-like approximation.[28] Again we point out that this approximation may lead to erroneous results.

Installations Plan. The Siloé reactor is operated by the Commissariat à l'Energie Atomique (CEA).

APPENDIX: EIGENVALUES AND EIGENSTATES OF THE CEF HAMILTONIAN

We list the eigenvalues and associated eigenstates of the CEF Hamiltonian in terms of the B_l^m parameters. We first define four intermediate parameters. We set $a_1 = -15120B_6^0 + 120B_4^0 - 24B_2^0$, $b_1 = \sqrt{140}(12B_4^4 + 360B_6^4)$, $a_2 = 11340B_6^0 + 900B_4^0 - 12B_2^0$, and $b_2 = \sqrt{7}(60B_4^4 - 180B_6^4)$. The eigenvalues are

$$E_{t1}^{(1)} = -10080B_6^0 + 960B_4^0 + 4B_2^0 - (a_1^2 + b_1^2)^{1/2}, \quad \text{(A1)}$$

$$E_{t1}^{(2)} = -10080B_6^0 + 960B_4^0 + 4B_2^0 + (a_1^2 + b_1^2)^{1/2}, \quad \text{(A2)}$$

$$E_{t2} = 5040B_6^0 + 840B_4^0 + 28B_2^0, \quad \text{(A3)}$$

$$E_{t3} = 27720B_6^0 - 660B_4^0 - 8B_2^0 - 180B_4^4 + 2520B_6^4, \quad \text{(A4)}$$

$$E_{t4} = 27720B_6^0 - 660B_4^0 - 8B_2^0 + 180B_4^4 - 2520B_6^4, \quad \text{(A5)}$$

$$E_{t5}^{(1)} = -10080B_6^0 - 360B_4^0 - 5B_2^0 - (a_2^2 + b_2^2)^{1/2}, \quad \text{(A6)}$$

$$E_{t5}^{(2)} = -10080B_6^0 - 360B_4^0 - 5B_2^0 + (a_2^2 + b_2^2)^{1/2}. \quad \text{(A7)}$$

We note the following relations:

$$E_{t1}^{(1)} - E_{t2} = a_1 - (a_1^2 + b_1^2)^{1/2} \quad \text{(A8)}$$

and

$$E_{t1}^{(2)} - E_{t2} = a_1 + (a_1^2 + b_1^2)^{1/2}. \quad \text{(A9)}$$

These relations mean that $E_{t1}^{(1)} \leqslant E_{t2} \leqslant E_{t1}^{(2)}$. In addition we have $E_{t5}^{(1)} \leqslant E_{t5}^{(2)}$.

The eigenstates are better written in terms of mixing angles because their normalization is then obvious. Other notations are not so transparent.[4] For that purpose we define two angles β_1 and β_2 through their tangent:

$$\tan\beta_i = \frac{(a_i + \sqrt{a_i^2 + b_i^2})}{b_i}. \quad \text{(A10)}$$

The eigenstate expressions are

$$|\Gamma_{t1}^{(1)}\rangle = 2^{-1/2}\sin\beta_1(|4\rangle + |-4\rangle) - \cos\beta_1|0\rangle, \quad \text{(A11)}$$

$$|\Gamma_{t1}^{(2)}\rangle = 2^{-1/2}\cos\beta_1(|4\rangle + |-4\rangle) + \sin\beta_1|0\rangle, \quad \text{(A12)}$$

$$|\Gamma_{t2}\rangle = 2^{-1/2}(|4\rangle - |-4\rangle), \quad \text{(A13)}$$

$$|\Gamma_{t3}\rangle = 2^{-1/2}(|2\rangle - |-2\rangle), \quad \text{(A14)}$$

$$|\Gamma_{t4}\rangle = 2^{-1/2}(|2\rangle + |-2\rangle), \quad \text{(A15)}$$

$$|\Gamma_{t5}^{(1)}\rangle = \sin\beta_2|\pm 3\rangle - \cos\beta_2|\mp 1\rangle, \quad \text{(A16)}$$

$$|\Gamma_{t5}^{(2)}\rangle = \cos\beta_2|\pm 3\rangle + \sin\beta_2|\mp 1\rangle. \quad \text{(A17)}$$

We notice that when analyzing data it is more practical and physical to consider the energy difference between the CEF levels and the two mixing angles than the B_l^m parameters.

[1] T. Shigeoka, N. Iwata, and H. Fujii, J. Magn. Magn. Mater. **104-107**, 1229 (1992).

[2] A. Blaise, B. Fåk, J. P. Sanchez, G. Amoretti, P. Santini, R. Caciuffo, D. Schmitt, B. Malaman, and G. Venturini, J. Phys.: Condens. Matter **7**, 8317 (1995).

[3] M. Slaski, A. Szytula, J. Leciejewicz, and A. Zygmunt, J. Magn. Magn. Mater. **46**, 114 (1984).

[4] P. Santini and G. Amoretti, Phys. Rev. Lett. **73**, 1027 (1994); C. Broholm, H. Lin, P. T. Matthews, T. E. Mason, W. J. L. Buyers, M. F. Collins, A. A. Menovsky, J. A. Mydosh, and J. K. Kjems, Phys. Rev. B **43**, 12 809 (1991).

[5] A. A. Moolenaar, P. C. M. Gubbens, and J. J. van Loef, Nucl. Instrum. Methods Phys. Res. B **94**, 555 (1994).

[6] I. A. Campbell, J. Phys. F **2**, L47 (1972).

[7] F. Baudelet, Ph.D. thesis, Paris-Orsay University, 1991.

[8] E. B. Karlsson, *Solid State Phenomena as Seen by Muons, Protons and Excited Nuclei* (Clarendon Press, Oxford, 1995); A. Schenck and F.N. Gygax, in *Handbook of Magnetic Materials*, edited by K.H.J. Buschow (Elsevier, New York, 1995), Vol. 9.

[9] A. Yaouanc, P. Dalmas de Réotier, P. C. M. Gubbens, A. A. Moolenaar, A. A. Menovsky, and C. E. Snel, Hyperfine Interact. **85**, 351 (1994).

[10] P. Wolfers, J. Appl. Crystallogr. **23**, 554 (1990).

[11] L. Koester, H. Rauch, and E. Seymann, At. Data Nucl. Data Tables **49**, 65 (1991).

[12] A. J. Freeman and J. P. Desclaux, J. Magn. Magn. Mater. **12**, 11 (1979).

[13] A. March, Z. Kristallogr. **81**, 285 (1932).

[14] And a preliminary INS experiment performed at the reactor of the Interfaculty Reactor Institute (Delft).

[15] M. T. Hutchings, Solid State Phys. **16**, 227 (1964).

[16] G. T. Trammell, Phys. Rev. **31**, 3625 (1963).

[17] B. Bleaney, Proc. R. Soc. London, Ser. A **276**, 19 (1963).

[18] J. Jensen and A.R. MacKintosh, *Rare Earth Magnetism, Structures and Excitations* (Clarendon Press, Oxford, 1991).

[19] See, for example, E. Bucher, C. W. Chu, J. P. Maita, K. Andres, A. S. Cooper, E. Buehler, and K. Nassau, Phys. Rev. Lett. **22**, 1260 (1969).

[20] W. L. Wang and B. R. Cooper, Phys. Rev. **172**, 539 (1968).

[21] W. L. Wang and B. R. Cooper, Phys. Rev. **185**, 696 (1969).

[22] D. A. Pink, J. Phys. C **1**, 1246 (1968).

[23] B. R. Cooper and O. Vogt, J. Phys. C **1**, 958 (1971).

[24] B. Chevalier, J. Etourneau, P. Hagenmuller, S. Quezel, and J. Rossat-Mignod, J. Less-Common Met. **111**, 161 (1985).

[25] D. Gignoux and D. Schmitt, Phys. Rev. B **48**, 12 682 (1993).

[26] Z. Zolnierek and J. Mulak, J. Magn. Magn. Mater. **140-144**, 1393 (1995).

[27] G. J. Nieuwenhuys, Phys. Rev. B **35**, 5260 (1987).

[28] A. E. Sikkema, W. J. L. Buyers, I. Affleck, and J. Gan, Phys. Rev. B **54**, 9322 (1996).